

Stress field evolution above the Peruvian flat-slab (Cordillera Blanca, northern Peru)

Audrey Margirier, L. Audin, X. Robert, A. Pêcher, S. Schwartz

▶ **To cite this version:**

Audrey Margirier, L. Audin, X. Robert, A. Pêcher, S. Schwartz. Stress field evolution above the Peruvian flat-slab (Cordillera Blanca, northern Peru). Journal of South American Earth Sciences, 2017, 77, pp.58-69. 10.1016/j.jsames.2017.04.015 . insu-01677069

HAL Id: insu-01677069

https://insu.hal.science/insu-01677069

Submitted on 16 Feb 2018

HAL is a multi-disciplinary open access archive for the deposit and dissemination of scientific research documents, whether they are published or not. The documents may come from teaching and research institutions in France or abroad, or from public or private research centers.

L'archive ouverte pluridisciplinaire **HAL**, est destinée au dépôt et à la diffusion de documents scientifiques de niveau recherche, publiés ou non, émanant des établissements d'enseignement et de recherche français ou étrangers, des laboratoires publics ou privés.

Stress field evolution above the Peruvian flat-slab (Cordillera Blanca, northern Peru)

A. Margirier[1], L. Audin[1], X. Robert[1], A. Pêcher[1], S. Schwartz[1]

[1]*Université Grenoble, Alpes, CNRS, IRD, ISTerre, F-38000 Grenoble, France*

Abstract

In subduction settings, the tectonic regime of the overriding plate is closely related to the geometry of the subducting plate. Flat-slab segments are supposed to increase coupling at the plate interface in the Andes, resulting in an increase and eastward migration of the shortening in the overriding plate. Above the Peruvian flat-slab, a 200 km-long normal fault trend parallel to the range and delimits the western flank of the Cordillera Blanca. In a context of flat subduction, expected to produce shortening, the presence of the Cordillera Blanca normal fault (CBNF) is surprising. We performed a systematic inversion of striated fault planes in the Cordillera Blanca region to better characterize the stress field above the Peruvian flat-slab. It evidences the succession of different tectonic regimes. NE-SW extension is predominant in most of the sites indicating a regional extension. We suggest that the Peruvian flat-slab trigger extension in the Western Cordillera while the shortening migrated eastward. Finally, we propose that flat-slab segments do not increase the coupling at the trench neither the shortening in the overriding plate but only favor shortening migration backward. However, the stress field of the overriding plate arises from the evolution of plate interface properties through time due to bathymetric anomaly migration.

Key-works

Inversion of striated fault planes; crustal stress field; mountain building; Peruvian flat-slab; Cordillera Blanca

1. Introduction

The western South American margin is segmented along-strike, with changing Andean topography and slab dip variations (*Barazangi and Isacks*, 1976). Two flat-slab segments have been identified by seismological data in northern Peru (3-15°S) and central Chile (28-32°S) (*Barazangi and Isacks*, 1976; Fig. 1). In such subduction settings, the tectonic regime of the overriding plate is closely related to the convergence direction, dip and geometry of the subducting plate (*Ramos and Folguera*, 2009). Around the world, flat-slab segments appear to increase coupling at the plate interface, resulting in both an increase and eastward migration of the shortening in the overriding plate (*Jordan et al.*, 1983; *Ramos and Folguera*, 2009; *Martinod et al.*, 2010).

Above the Peruvian flat-slab, a striking 200 km-long normal fault trending parallel to the range delimits the western flank of the Cordillera Blanca high peaks (*Bonnot*, 1984; *McNulty and Farber*, 2002; *Giovanni*, 2007). Those peaks (>6000 m) are abnormally higher than the average plateau altitude at this place (~4400 m). In such a context of flat subduction, expected to produce shortening, the joint presence of the Cordillera Blanca normal fault (CBNF) with high reliefs is surprising. Indeed, despite regional expected shortening related to the flat-slab subduction of the Nazca Plate beneath the South America, the Cordillera Blanca normal fault has been active during the Quaternary. Two models have been proposed to explain the occurrence of extension in this part of the high Andes: *Dalmayrac and Molnar* (1981) suggested an extensional collapse of a thickened crust, whereas *McNulty and Farber* (2002) involved oceanic ridge buoyancy under the Cordillera Blanca. Despite these models, the tectonic setting of the Cordillera Blanca emplacement is still debated: while *Petford and Atherton* (1992) suggested that the Cordillera Blanca batholith has emplaced in a dextral

52 wrench regime based on ductile deformation structures, *McNulty et al.* (1998) interpreted
53 some magnetic susceptibility data from the batholith as the result of a sinistral wrench regime.
54 As this opposition extension versus along strike shearing is a key issue for Andean
55 geodynamics (e.g., *Dewey and Lamb*, 1992; *McNulty et al.*, 1998; *Taylor et al.*, 1998;
56 *Scheuber and Gonzalez*, 1999; *Folguera et al.*, 2006, *Audin et al.*, 2008), the aim of this paper
57 is to precise and constrain the stress field evolution through time in this region with new
58 microstructural data. Indeed, analyzing the ductile and brittle tectonic deformation in the crust
59 permits to describe the impact of flat subduction on the stress field in the overriding plate in
60 northern Peru. Moreover, the knowledge of the regional stress field evolution could provide
61 information on processes driving the Cordillera Blanca batholith exhumation. The stress field
62 evolution above the flat-slab is mainly inferred from inversions of striated fault planes
63 measured on different outcrops in the Cordillera Blanca region.
64

65 **2. Geodynamic and tectonic context of northern Peru**

66 **2.1. Geodynamic setting**

67 The Andes are the result of the long-lasting subduction of the Nazca Plate beneath the South
68 America Plate. The subduction zone has been active since at least Cretaceous time, with
69 convergence rates, obliquity and subduction dip changing through time (e.g., *Somoza*, 1998;
70 *Ramos and Folguera*, 2009; *Martinod et al.*, 2010). These changes have been associated to
71 different tectonic phases affecting the Andean range (e.g., *Jordan et al.*, 1983; *Pardo-Casas*
72 *and Molnar*, 1987; *Somoza*, 1998) and influenced the magmatic activity along strike (*Kay and*
73 *Kay*, 2002; *Ramos and Folguera*, 2009).
74 The northern Peruvian margin displays a present-day flat subduction zone where both, the
75 geometry and timing of slab flattening are well constrained for the last 15 Ma (e.g., *Gutscher*
76 *et al.*, 1999; *Hampel*, 2002; *Rosenbaum et al.*, 2005; *Antonijevic et al.*, 2015). *Gutscher et al.*
77 (2000) suggested that the flat-slab has a ~20 km deep sag between the Nazca Ridge and the

78 Inca Plateau thickened parts (Fig. 1). The subduction of these two buoyant features have been
79 proposed to induce the slab flattening in northern Peru (*Gutscher et al.*, 1999). Based on this
80 hypothesis, several reconstructions of the timing and location of the initial Nazca Ridge
81 subduction based on symmetric seafloor-spreading in a hotspot reference frame constrained
82 the timing of the slab flattening (e.g., *Hampel*, 2002; *McNulty and Farber*, 2002; *Rosenbaum*
83 *et al.*, 2005; *Antonijevic et al.*, 2015). However, all of these models rely on calculations of the
84 motion of the Nazca Plate with respect to South America, which may induce considerable
85 errors. *Rosenbaum et al.* (2005) presented a regionally refined plate circuit that suggests the
86 initiation of the Nazca Ridge subduction at 15 Ma at 10°S and the arrival of the Inca Plateau
87 at 13 Ma at 5°S. This reconstruction, in agreement with the timing of magmatism migration
88 eastward, indicates that the slab flattening occur at the latitude of the Cordillera Blanca region
89 from ~15 Ma.
90
91 **2.2. Peruvian tectonic history**
92 Several tectonic phases corresponding to short tectonic events that seems to have largely
93 contributed to the Andean range building have been identified (*Mégard*, 1984). The first
94 known major compressional event occurred in Late Albian, (113.0-100.5 Ma; *Mégard*, 1984).
95 This tectonic phase, named Mochica, is recorded in the whole Western flank of the Central
96 Andes (*Jaillard*, 1994) and is characterized by NE-SW compression (*Mégard*, 1984) likely
97 associated with a dextral wrenching component (*Bussel and Pitcher*, 1985). It has been
98 followed by a widespread episode of deformation in Peru, named the Peruvian phase, during
99 the Santonian and the Campanian (86.3-70.6 Ma, NE-SW compression; *Steinmann*, 1929;
100 *Mégard*, 1978; *Gayet et al.*, 1991, *Jaillard et al.*, 1993; *Jaillard and Soler*, 1996). An episode
101 of uplift is likely contemporaneous with Peruvian phase in the Western Cordillera (*Mégard*,
102 1984). Then, from mid to late Eocene the main Andean shortening phase, the Incaic phase,
103 caused extensive folding and reverse faulting in the Jurassic sediments of the Western

104 Cordillera and the formation of a fold and trust belt along the Western Cordillera in Central
105 Andes (48.6-33.9 Ma, NE-SW compression; *Mégard*, 1984; *Noble et al.*, 1990).

106 The Neogene tectonic phase named the Quechua phase is divided in three discrete phases
107 (e.g., *McKee and Noble*, 1982; *Mégard*, 1984). The Quechua 1 phase (20-12.5 Ma) is
108 characterized by NW-SE shortening and by reactivation of structures inherited from the Incaic
109 phase in northern Peru, from the Western Cordillera to farther east. It seems that the
110 deformation associated with the Quechua 1 phase reached the Eastern Cordillera (*Mégard*,
111 1984). The Quechua 2 is bracketed between 9.5 and 8.2 Ma in central Peru (*Mégard et al.*,
112 1984). This phase is characterized by dextral strike-slip along NW-SE structures likely caused
113 by N-S compression (*Soulas*, 1977). Finally, the Quechua 3 phase identified in the subandean
114 fold and thrust belt (~6 Ma; *Mégard*, 1984) is characterized by E-W compression (*Soulas*,
115 1977).

116

117 **2.3. Geologic and Quaternary tectonic settings of the Cordillera Blanca region**

118 The Cordillera Blanca and the Cordillera Negra are located in the northern Peruvian Andes, in
119 the Western Cordillera (Fig. 1). The Cordillera Blanca is a Miocene granitic pluton (14-5 Ma;
120 *Mukasa*, 1984; *McNulty et al.*, 1998; *Giovanni*, 2007) emplaced in deformed Jurassic
121 sediments of the Chicama Formation at pressures ranging from 100 to 200 MPa (*Petford and*
122 *Atherton*, 1992; *Margirier et al.,* 2016). The Cordillera Blanca batholith and associated
123 magmas, the Fortaleza and Yungay ignimbrites emplaced respectively around 7.4 Ma (*Wipf*,
124 2006) and between 8 and 3 Ma (*Wise and Noble*, 2003; *Giovanni*, 2007; *Giovanni et al.*,
125 2010), correspond to the last magmatic activity before the cessation of magmatism associated
126 to the slab flattening in northern Peru (*Petford and Atherton*, 1992).

127 The high summits of the Cordillera Blanca correspond to the footwall of the CBNF. The
128 elongated shape (trending parallel to the Andean range) and the internal fabric of the batholith
129 suggest its emplacement along a pre-existing lithospheric fault structure, in a strike-slip

130 context (*Cobbing et al.*, 1981; *Petford and Atherton*, 1992; *McNulty et al.*, 1998). However,
131 there is no consensus about the kinematics: dextral (based on ductile sub-solidus fabric in the
132 granite and on en-echelon structure in pegmatites; *Petford and Atherton*, 1992) versus
133 sinistral (from unclear AMS fabric; *McNulty et al.*, 1998).
134 Preliminary studies addressed the Cordillera Blanca brittle tectonic history with microtectonic
135 data and stress reconstructions from fault slip dataset inversion (*Bonnot*, 1984; *Sébrier et al.*,
136 1988). *Bonnot* (1984) proposed the succession of the following tectonic phases: (I) Pliocene
137 E-W extension (σ_3 sub-horizontal N285, σ_1 sub-vertical), (II) Quaternary E-W compression
138 (σ_1 sub-horizontal N080, σ_3 sub-vertical) and N-S compression (σ_1 sub-horizontal N150, σ_3
139 sub-vertical), (III) N-S extension from the Pleistocene to present day (σ_3 sub-horizontal N0,
140 σ_1 sub-vertical). *Sébrier et al.* (1988) only focused on the last fault slip and suggested N-S
141 extension in the Cordillera Blanca. Neither the Quaternary compression nor the N-S extension
142 they evidenced in the Cordillera Blanca is in agreement with present day extensional
143 microseismicity (*Deverchère et al.*, 1989).

144 The general trend of the Cordillera Blanca fault zone is N140° dipping 35-45°SW. Variations
145 of the scarp heights and en echelon faulting in the southern part of the fault show that the
146 CBNF is segmented (Fig. 2; *Giovanni*, 2007). Field studies evidence discontinuous NW-SE
147 striking scarps that displace Quaternary glacial moraines as well as plutonic rocks (Fig. 3;
148 e.g., *Bonnot*, 1984; *Schwartz*, 1988). Along the fault zone, repeated displacements imprinted
149 the landscape, with ~2 to >100 m-high scarps, corresponding to vertical displacements
150 cumulated during the Quaternary (Fig. 3B, C) and ~1 km-high triangular facets (Fig. 3A). In
151 total, considering the emplacement depth of the Cordillera Blanca batholith, the scarps height
152 and the basin sedimentary filling thickness, the CBNF shows at least 4500 m of vertical
153 displacement in its central part since ~5 Ma (*Bonnot*, 1984; *Giovanni*, 2007; *Margirier et al.*,
154 2016).
155 Based on thermochronologic data (apatite fission-tracks and apatite (U-Th)/He), *Giovanni*

156 (2007) and *Hodson* (2012) gave estimation of exhumation rate at ~2 mm/yr and >1 mm/yr
157 respectively on the central part of the CBNF and decreasing exhumation rates toward the
158 South for the last 3 Ma. For the last 4 Ma, *Margirier et al.* (2015), based on the same
159 thermochronologic systems, suggest lower exhumation rate (1 mm/yr) for the central part of
160 the Cordillera Blanca. Even if modeling of thermochronologic ages did not indicate a well-
161 defined north-south trend in erosion rate (*Margirier et al.*, 2016) the total exhumation since
162 the batholith emplacement decreases in the southern part of the Cordillera Blanca (*Margirier*
163 *et al.*, 2016). Based on the CBNF morphology and the Cordillera Blanca geology *Bonnot*
164 (1984) estimated vertical slip rates of ~0.7 mm/yr on the CBNF between 3 and 0 Ma. On a
165 more recent time scale (30-0 ka), the CBNF displacement rates have been constrained by ^{10}Be
166 dating of scarps (*Siame et al.*, 2006) and geomorphic features (moraines) displaced by the
167 fault (Fig. 3B, C; *Schwartz*, 1988; *Farber and Hancock*, in prep). The vertical slip rates
168 decrease from north to south ranging from 5.1 ± 0.8 mm/yr to 0.6 ± 0.2 mm/yr (Fig. 2B;
169 *Schwartz*, 1988; *Siame et al.,* 2006; *Farber and Hancock,* in prep).
170 In terms of seismic activity, no historical earthquake has been reported for the CBNF
171 (*Silgado*, 1992). However, some microseismicity occurs in the Cordillera Blanca region. The
172 focal mechanisms indicated present-day NE-SW extension in adequacy with Quaternary
173 offsets along the CBNF (*Deverchère et al.*, 1989). The most significant coseismic surface
174 faulting has been reported in 1946 along the Quiches normal fault (Mw = 6.8; *Doser*, 1987;
175 *Bellier et al.*, 1991), 50 km north-east from the CBNF trace. No significant seismic event
176 (Mw>4) has been reported South of the CBNF segments neither along the Cordillera
177 Huayhuash neither farther South (Neotectonic Open Database[1]).

178 West of the Cordillera Blanca, the Callejón de Huaylas, an elongated range-parallel intra-
179 mountain basin (150 km long), builds the hanging wall of the CBNF and separates the
180 Cordillera Blanca and the Cordillera Negra. The sedimentary series filling this intra-mountain

[1] neotec-opendata.com

basin recorded its subsidence associated to the CBNF initiation and activity (*Bonnot*, 1984). Indeed, at the base of the series some ignimbrites dated at 5.4 ± 0.1 Ma suggest that normal faulting initiated at least at ~5.4 Ma (*Giovanni*, 2007, *Giovanni et al.*, 2010). Westward, the Cordillera Negra consists of Cretaceous and Paleogene plutons (73-48 Ma; *Mukasa*, 1984; *Beckinsale et al.*, 1985) intruded in the Chicama formation. Neogene volcano-sedimentary deposits capped the older formations in the southern part of the Cordillera Negra.

3. Methods

3.1. Satellite image analysis

In mountain ranges, the landscapes are largely controlled by the lithology and tectonic structures. Fracturing favors chemical weathering and weaken the rocks. Satellite imageries can be used to map fractures at up to kilometers scale in rocky landscapes/areas. Here, we analyzed satellite images (Google Earth, Landsat images, 2001-2002, visible band with a space resolution of 15 m) to map the main faults at regional/km scale (Fig. 2). Mapping displacements along active faults is based on displacement of surfaces or geomorphic markers such as moraines or Quaternary pediment surfaces. For each lineament we checked if it corresponds to a fault and not to a fold axis or a stratigraphy boundary (Fig. 2). To discuss the contradictory conclusions of previous works on the ductile deformation in the Cordillera Blanca (*Petford and Atherton*, 1992; *McNulty et al.*, 1998), we also collected ductile deformation data in the field and from satellite image (Google Earth, Landsat images; Fig. 4).

3.2. Tectonic stress inversion

3.2.1. Principe

Several methods, based on sets of fault planes and slickenlines, permit to estimate paleostress tensors (e.g., *Angelier and Mechler*, 1977; *Angelier*, 1984). The reduced stress tensor, obtained from faults-slickenlines pairs inversion, provides the orientation of the principal

stress axes σ_1, σ_2, σ_3 (with $\sigma_1 > \sigma_2 > \sigma_3$ and compression being positive) and a shape parameter that we defined here as *Phi* = $(\sigma_2 - \sigma_3)/(\sigma_1 - \sigma_3)$ (e.g., *Angelier*, 1984; *Delvaux and Sperner*, 2003). These inversion methods rely on three assumptions: (a) the stress is uniform in the volume of rock considered, (b) the stress tensor is equivalent to the incremental deformation tensor as obtained from the slip data, and (c) the slip vector on a fault plane (given by the slickenlines) is parallel to the maximum shear stress along the plane as deduced from the stress tensor (*Bott*, 1959). These assumptions imply careful choice of the measurement stations, and brittle deformation measurements.

3.2.2. Fieldwork

We measured more than 400 couples fault-slickenline on 38 sites in the Cordillera Blanca region (Table 1). For each site we measured between 2 and 34 striated fault planes (supplementary tables A1 and A2, for all the planes we measured dip direction and dip angle) on outcrops no larger than 50 m with homogenous lithology. We measured all the striated planes we have been able to see on the outcrops without selection. We constrained the displacement direction and sense on each fault plane with classical tectoglyphs (fibers, striations, steps…). For each measurement we attributed a qualitative confidence level for the sense of the displacement found on the field (supplementary table A2). We kept only the striated planes with unambiguous displacement sense. For “natural” outcrops, fault planes are weathered and the slickenlines are not well preserved, leading to too few measurements to be able to use them for analysis. Most of our sites are located along roads for quality of outcroppings: it is constituted of fresh rocks and most of the faults-planes and slickenside striae sets can be measured (orientation and dip). Measurement sites are mostly located in the Cordillera Blanca but few stations are in the Cordillera Negra and the Callejón de Huaylas (Fig. 2). This heterogeneous sampling is related to difficulties to find sites with competent, fractured and low weathered rocks in the Cordillera Negra.

234 ***3.2.3. Inversion methods***

235 Different computer softwares are available to determine the reduced stress tensor that best
236 explains the slip distribution on a set of fault planes (e.g., TectonicsFP, FaultKinWin,
237 TENSOR, WinTensor, Mim; *Marrett and Allmendinger*, 1990; *Sperner et al.*, 1993; *Yamaji*,
238 2000; *Ortner et al.*, 2002; *Delvaux and Sperner*, 2003; *Delvaux*, 2012). As they are based on
239 the same physical concepts, all these methods are expected to give similar results (*Delvaux*
240 *and Barth*, 2010; *Lacombe*, 2012). The inversion of the data was here performed using the
241 software WinTensor (*Delvaux*, 2012) which inverts a dataset with the right dihedra method
242 (*Angelier and Mechler*, 1977) and the PBT method (*Angelier*, 1984). In the right dihedra
243 method an auxiliary plane is defined, orthogonal to the striated plane and to the striae. The
244 striated plane and the auxiliary plane define 4 right dihedras and 2 half spaces: a shortening
245 half-space and an extensional half-space, defined by the kinematic of the striaes. All results
246 are then superimposed and a statistical outline is used to calculate a tensor with σ_1 in dihedra
247 in compression and σ_3 in dihedra in extension. This initial result is used by the "Rotational
248 Optimisation" procedure that minimizes, by an iterative grid search, the misfit angle (*Delvaux*
249 *and Sperner*, 2003). Based on *Wallace* (1951) and *Bott* (1959) principles, the PBT method
250 considers that the slip vector on a fault plane is parallel to the maximum shear stress along the
251 plane. For each striated plane, compression and extension axis (P and T-axis) are constructed,
252 both lying in the plane given by the shear plane normal and the slickenline. In homogeneous
253 materials, σ_2 lies in the fault plane, and σ_1 and σ_3 in the plane containing the fault-plane
254 normal and the striae.

255 The inversion requires at least 5 fault-slickenline pairs. A higher number of data better
256 constrains the solution. Here, we used at least 6 pairs of fault-slickenline for an inversion. The
257 angular misfit between the measured slickenline and the theoretical slickenline predicted from
258 the calculated tensor is used as a quality indicator of the inversion (Fig. 5).

259 We processed the data following a multistep approach (*Zeilinger et al.*, 2000). A random
260 tensor search was performed for each site (or grouped sites). The data is rejected when the

misfit between the slickenline and the theoretical slickenline predicted from the calculated tensor is >30°. Then, all the rejected striated planes are recovered and the same procedure was applied. Populations of less than 6 striated planes were considered not significant. For each valley when our sites are close to each other (stations distributed in an area smaller than 10 km), we group the sites located in tectonically homogeneous units to process them as single sites and average the regional stress field (*Zeilinger et al.*, 2000; *Pêcher et al.*, 2008). The larger number of fault-slickenline pairs for grouped sites permits a more robust determination of tensors.

4. Results

4.1. Ductile deformation and local cooling ages of the Cordillera Blanca batholith

We analyzed punctual ductile deformation evidences during the fieldwork and from satellite images to discuss the tectonic context during the Cordillera Blanca batholith emplacement. The granitic veins developed in the sediments close to the batholith contact are good deformation markers ranging from field to satellite scale. Their ductile deformation provides a reliable constraint of the upper plate regional strain axes contemporary of their emplacement.

Along the eastern limit of the Cordillera Blanca batholith, some deformed dykes intruded the Jurassic sediments and indicates a dextral sense of shearing along the batholith (Fig. 2 and 4A). The surrounding granite is dated at ~8 Ma (zircon U-Pb and muscovite Ar-Ar; *Giovanni*, 2007).

In the Cordillera Blanca batholith a penetrative foliation and S-C structures indicates normal top to SW sense of shearing. In addition, in the Canyon del Pato close to the contact between the batholith and sediments, a dyke complex intrudes sedimentary rocks of the Chicama Formation. Its ductile deformation indicates normal top to SW sense of shearing and NE-SW extension (shearing plane = N145 30SW, stretching lineation = N50 20SW; Fig. 4B). Close to this outcrop, the Cordillera Blanca batholith cooling is younger, ages range from 5 to 3.6 Ma (muscovite Ar-Ar and K-Ar; *Stewart et al.*, 1974; *Giovanni*, 2007).

4.2. Brittle deformation

4.2.1. The Cordillera Blanca normal fault

Along strike the fault displays a well-defined scarp developed either in the bedrock, in Quaternary alluvial fan, moraines or debris-flow deposits attesting of repeated displacements. Field surveys evidence cumulative scarp height decreasing in lower and younger deposits, it suggests multiple Holocene faulting events preserved on each sites. Southwards, the Holocene fault scarp varies from a well-defined single scarp tens m-high to several sub-parallel en echelon faulting of about 1 m-high. Punctually, the fault trace splits down in the Callejon de Huaylas into small graben and antithetic scarps, adjacent to the main scarp (Fig. 2). Northwards, the Quaternary scarp (strike N140°) displays an impressive and constant westward dip of ~35 to 45°.

Along the CBNF several sites display striaes on the fault plane: from North to South, in Pachma Bajo, Quebrada Llaca and Quebrada Querococha (Fig. 2B). Striae on the fault have a down dip direction (N249-39SW). Tectoglyphs indicate a normal sense displacement (Fig. 5) consistent with the Quaternary displacement of the moraines along the CBNF (*Dalmayrac and Molnar*, 1981; *Bonnot*, 1984). This normal fault accommodates an ENE-WSW extension. *Bonnot* (1984) also reports bedrock slickensides along the fault scarp between Chiquian and Huaraz. He suggested that there might have been a sinistral component to the Quaternary slip on the fault segments striking N110 to N155. The en-echelon faults striking N140 in the southern part of the CBNF also suggest a sinistral component (*Bonnot*, 1984). However, the cumulated amount of such strike-slip component must be negligible because lateral offsets of moraine axes are not observed on the field.

4.2.2. Example of a multistep deformation history in the Canyon del Pato

In the Canyon del Pato, we collected data from 5 sites spread along a 5 km-distance. All the sites are located in the Cordillera Blanca batholith close to the CBNF (Fig. 2). We measured

315 in this area 128 fault-slickenline pairs in the Neogene bedrock (Fig. 6). Here, a single stress
316 tensor cannot explain our data; the angular deviation is > 50° for ~50% of the data. The
317 important dispersion of fault orientations (Fig. 6) suggests a multistep brittle deformation
318 history. Following this hypothesis, we obtained 3 stress tensors from faults-slickenlines
319 inversion. Labeling T1, T2 and T3 refer only to the number of striated planes associated to
320 each tensor and didn't imply a chronology. The predominant tensor (T1, 66 faults)
321 corresponds to NE-SW pure extension (Fig. 6). The second stress tensor (T2, 12 faults) is
322 related to E-W transpression with a component in sinistral strike-slip. The less well-defined
323 third stress tensor (T3, 11 faults) corresponds to E-W pure extension. None of the T3 axes is
324 vertical indicating that this tensor has been tilted while T1 and T2 seem not tilted. It could
325 indicate that T3 is the older tensor.
326
327 ***4.2.3. Regional stress fields***
328 Most of our measurements were taken in the Cordillera Blanca batholith. In addition, five
329 sites are located in the southern part of the Cordillera Blanca (Quebrada Pastoruri), in
330 sedimentary and volcanic rocks, one is in the Callejón de Huaylas (Caraz) and two sites are
331 located in the Cordillera Negra (Fortaleza Valley and Pueblo Libre). The results of stress
332 tensors for grouped sites are presented in the Table 1. For the best-defined tensor (T1) most of
333 the misfit are lower than 15° demonstrating the quality of the inversion, for the other tensors
334 (T2 and T3) most of the misfit are lower than 20°.
335 The Cordillera Blanca brittle deformation reflects the recent stress field that is superimposed
336 on ductile deformation acquired during the Cordillera Blanca emplacement and early
337 exhumation. In most of the sites we found up to two tensors with different characteristics
338 (extension, wrenching and compression). The wide range of tensors suggests a multistep
339 brittle deformation history in the Cordillera Blanca region. The best-expressed stress tensor
340 corresponds to NE-SW extension (80% of the 38 sites; Figs. 7, 8A). The extension is not
341 restricted to the Cordillera Blanca. Indeed, the Pueblo Libre and the Fortaleza sites recorded

342 respectively E-W extension and transtension with horizontal E-W σ_3 axis. The stress
343 inversion also indicates wrenching (50% of the sites), N-S extension (in Quebradas Ulta,
344 Querococha and Pastoruri, 30% of the sites) and E-W compression (in Quebradas Llaca and
345 Ulta, 15% of the sites) (Figs. 7, 8). The E-W compression tensors indicate that a
346 compressional phase affect the Cordillera Blanca region after the Cordillera Blanca
347 emplacement. Therefore, after ~8 Ma several tectonic regimes followed one another in the
348 Cordillera Blanca region.
349

350 **5. Discussion**

351 **5.1. Tectonic context for the Cordillera Blanca emplacement**

352 Our ductile deformation data indicates two different strain regimes: a dextral strike-slip in the
353 eastern part of the Cordillera Blanca (Fig. 4A, see Fig. 2 for site location) and an E-W
354 extension close to the CBNF, in the northern part of the Cordillera Blanca (Fig. 4B). As the
355 Cordillera Blanca batholith displays different ages in these two sites and as the deformation
356 indicates two different strain regimes, these two regimes may result from different tectonic
357 phases.

358 First, the granite emplaced in a dextral strike-slip regime (~8 Ma, Fig. 4A). Our data are here
359 in agreement with the ductile deformation evidenced by *Petford and Atherton* (1992). This
360 dextral strike-slip likely corresponds to a late stage of the Quechua 2 tectonic phase (9.5-8.5
361 Ma) which is characterized by strike-slip movements on NW-SE faults resulting from N-S
362 compression (*Mégard*, 1984; *Mégard et al.*, 1984).

363 Close to the CBNF the ductile deformation recorded NE-SW extension (Fig. 4B). In this area
364 the batholith is young ~4.5 Ma (*Stewart et al.*, 1974; *Giovanni*, 2007); this NE-SW extension
365 exists at least since the Cordillera Blanca batholith emplacement and is consistent with the
366 initiation of the Callejón de Huaylas subsidence at ~5.4 Ma associated to the CBNF activity
367 (*Bonnot*, 1984; *Giovanni*, 2007).
368

369 **5.2. Chronology of the different stress field imprinted in the Cordillera Blanca batholith**

370 The Cordillera Blanca region recorded two steps of ductile deformation and a multistep brittle
371 deformation history. The identified stress fields are: NE-SW extension, N-S extension, E-W
372 compression and ~E-W transtension (Table 1, Figs. 6, 8). Despite numerous markers of
373 superposed movements on fault planes their relative chronology was unclear. It is not possible
374 to reconstruct the chronology of stress field based on field criteria. Therefore, we compare
375 calculated stress tensor with tectonic phases documented by *Mégard* (1984) in northern Peru
376 and with the present day stress field inferred from microseismicity (*Deverchère et al.*, 1989).
377 The ductile deformation indicates a dextral strike-slip at ~8 Ma in the eastern part of the
378 Cordillera Blanca. This deformation could be related to the Quechua 2 period, which has
379 produced dextral strike-slip on NW-SE trending faults in Ayacucho basin between 9.5 and 8.5
380 Ma (*Mégard et al.*, 1984). Then, the ductile NE-SW extension observed in the Canyon del
381 Pato (~5 Ma) likely corresponds to the earlier brittle deformation NE-SW extensional tensors.
382 This extension posterior to ~4.5 Ma is in agreement with the initiation of the CBNF at ~5.4
383 Ma (*Bonnot*, 1984). Moreover, this NE-SW extension is similar to the regional stress tensor
384 deduced from a microseismicity survey (*Deverchère et al.*, 1989). Thus, we suggest that these
385 ductile and brittle deformation phases are related to a state of stress identical to state of stress
386 observed at the present day in the Cordillera Blanca region. This state of stress was effective
387 regionally at least for the last ~5 Ma. The extensional stress tensors are not restricted to the
388 Cordillera Blanca. It likely corresponds to a large-scale process driving extension in the
389 overriding plate.
390 In addition, the less-expressed stress tensors indicate locally some anomalies in the stress
391 field. Indeed the brittle deformation also indicates that E-W compression episode in the
392 Cordillera Blanca batholith. This compressional episode is also recorded in the Callejón de
393 Huaylas basin (*Bonnot*, 1984). It could be related to the Pliocene Quechua 3 compressional
394 phase (*Mégard*, 1984) which could have trigger a brief compressional phase during the CBNF
395 activity (since ~5.4 Ma). Finally, the brittle deformation also recorded multidirectional

396 extension (*Phi* < 0.5) in the Cordillera Blanca (Quebrada Paron, Quebrada Querococha,
397 Quebrada Pastoruri). This stress field could be related to the Quaternary rapid exhumation of
398 the central part of the Cordillera Blanca (*Margirier et al.*, 2016).
399
400 **5.3. Different tectonic phases above the Peruvian flat-slab**
401 This study evidence the occurrence of several tectonic phases above the Peruvian flat-slab
402 segment during the past 8 Myr in agreement with *Bonnot* (1984). These successive tectonic
403 phases and the occurrence of predominant extension perpendicular to the trench suggest that
404 flat-slab segments do not always induce compression in the upper plate as previously
405 suggested (*Jordan et al.*, 1983; *Ramos and Folguera*, 2009; *Martinod et al.*, 2010). The
406 tectonic regime changes may be associated to other parameters as plates velocities, plates
407 directions, the absolute movement of the trench, the age of the oceanic plate, the presence of
408 sediments or the geometry of the oceanic plate (e.g., *Ruff and Kanamori*, 1983; *Heuret et al.*,
409 2007; *Schellart*, 2008). As the tectonic regime change occurs in a short period of time it could
410 be linked to a local process (versus a large scale geodynamic process). The Peruvian flat slab
411 geometry includes two thickened parts, the Nazca Ridge and the Inca Plateau, and a sag
412 between these two features (*Gutscher et al.*, 1999). Plate reconstructions indicated that the
413 Nazca Ridge subduction initiate at ~10°S at ~15 Ma and then the ridge migrate southward
414 (*Hampel*, 2002; *Rosenbaum et al.*, 2005; *Antonijevic et al.*, 2015). The subduction of the
415 Nazca Ridge below the Cordillera Blanca could have induced an increase of the coupling
416 (e.g., *Gutscher et al.*, 2000; *McNulty and Farber*, 2002; *Martinod et al.*, 2010) and triggered
417 compressional stress field in this area. After the migration of the ridge toward the South when
418 the sag arrived below the Cordillera Blanca, the coupling could have decreased and permitted
419 extension in the overriding plate. Indeed, *Nocquet et al.* (2014) demonstrated that the
420 subduction segments of northern Peru show a low to weak interseismic coupling contrasting
421 with the southern Peru region. Similarly, above the Mexican flat-subduction, *Gérault et al.*
422 (2015) suggested the control of the mantle dynamic and of a weak subduction interface in the

423 "neutral" state of stress. Finally, all flat slab segments do not trigger extension. For example,
424 no extension have been reported above the Pampean flat-slab in Chile (e.g., *Ramos et al.*,
425 2002), whereas the Nazca Plate have the same age and dip in these two segments (*Barazangi*
426 *and Isacks*, 1976; *Müller et al.*, 2008). The presence of an over-thickened crust (~50 km,
427 *James*, 1971) in Peru could favor extension independently of subduction properties
428 (*Froidevaux and Isacks*, 1984). In addition, the amount of sediments on the oceanic plate is
429 different in Peru and Chile: The sediment thickness reaches ~500 m in Peru, in Chile there is
430 no sediments (*Divins*, 2006). The presence of sediment can change the plate interface
431 properties (*Ruff*, 1989). Indeed, in Peru GPS survey suggest the subduction interface is not
432 homogeneously coupled along-strike with the existence of a ~500 km-long uncoupled
433 segment in northern Peru whereas in southern Peru and Chile the subduction interface is
434 characterized by highly coupled asperities separated by narrower zones of low interseismic
435 coupling (*Nocquet et al.*, 2014; *Saillard et al.*, 2017).
436
437 **6. Conclusions**
438 Our data suggest a complex tectonic history in the Cordillera Blanca region. The analysis of
439 ductile deformation in the eastern part of the Cordillera Blanca batholith (8 Ma) suggests that
440 the batholith emplaced in a dextral strike-slip context according to *Petford and Atherton*
441 (1992) observations. In a younger part of the Cordillera Blanca batholith (~4.5 Ma) the ductile
442 deformation indicates NE-SW extension. Then, the multistep deformation recorded in the
443 Cordillera Blanca indicated the succession of different tectonic regimes (dextral strike-slip,
444 NE-SW extension, E-W compression and NE-SW extension) above the Peruvian flat-slab.
445 The presence of the crustal-scale CBNF and our NE-SW extensional stress tensor suggest that
446 flat subduction can trigger extension in the Western Cordillera while in the Eastern Cordillera
447 the shortening migrate eastward (*Mégard*, 1984). The extension may be facilitated by the
448 presence of a thickened crust in Peru (*Froidevaux and Isacks*, 1984), an absolute movement
449 of the overriding plate toward the trench or by a decrease of the convergence rate and a low

coupling at the plate interface (*Somoza*, 1998; *Nocquet et al.*, 2014). In the context of the long-lasting subduction of the Nazca Plate, we suggest that the change of tectonic regime in the overriding plate (from compression to extension) and the extension along the CBNF are likely associated to a decrease of the coupling at the plate interface at the trench and below the Western Cordillera while the shortening migrates eastwards. Finally, considering the occurrence of extension along the CBNF since 5.4 Ma and the predominant NE-SW extension regime, we suggest that flat-slabs do not always favor shortening in the overriding plate. The Peruvian flat-slab seems to not increase the coupling at the trench but only increase the coupling eastward and favor shortening migration in the subandean region.

Acknowledgments

This work was supported by a grant from LabEx OSUG@2020 (Observatoire des Sciences de l'Univers de Grenoble, Investissements d'Avenir, ANR10 LABX56), and SMINGUE. We thank the SERNAMP for allowing access to the Cordillera Blanca National Park. We acknowledge the editor, C. Costa and the anonymous reviewer for their constructive comments of this manuscript.

References

Angelier, J. (1984), Tectonic analysis of fault slip data sets, *Journal of Geophysical Research: Solid Earth*, *89*(B7), 5835–5848.

Angelier, J., and P. Mechler (1977), Sur une methode graphique de recherche des contraintes principales également utilisables en tectonique et en séismologie: la méthode des dièdres droits, *Bulletin de la Société Géologique de France*, *19*(6), 1309–1318.

Antonijevic, S. K., L. S. Wagner, A. Kumar, S. L. Beck, M. D. Long, G. Zandt, H. Tavera, and C. Condori (2015), The role of ridges in the formation and longevity of flat slabs, *Nature*, *524*(7564), 212–215, doi:10.1038/nature14648.

Audin, L., P. Lacan, H. Tavera, and F. Bondoux (2008), Upper plate deformation and seismic barrier in front of Nazca subduction zone: The Chololo Fault System and active tectonics along the Coastal Cordillera, southern Peru, *Tectonophysics*, *459* (1-4) 1, 174-185, doi:10.1016/j.tecto.2007.11.070.

Barazangi, M., and B. L. Isacks (1976), Spatial distribution of earthquakes and subduction of

481 the Nazca plate beneath South America, *Geology*, *4*(11), 686–692.

482 Beckinsale, R. D., A. W. Sanchez-Fernandez, M. Brook, E. J. Cobbing, W. P. Taylor, and N.
483 B. Moore (1985), Rb-Sr whole rock isochron and K-Ar determination for the Coastal
484 Batholith of Peru, in *Magmatism at a Plate Edge: The Peruvian Andes*, edited by W. S.
485 Pitcher, M. P. Atherton, E. J. Cobbing, and R. D. Beckinsale, pp. 177–202, Blackie
486 Halstead press, Glasgow.

487 Bellier, O., J. F. Dumont, M. Sébrier, and J. L. Mercier (1991), Geological constraints on the
488 kinematics and fault-plane solution of the quiches fault zone reactivated during the 10
489 November 1946 Ancash earthquake, northern Peru, *Bulletin of the Seismological Society*
490 *of America*, *81*(2), 468–490.

491 Bonnot, D. (1984), Néotectonique et tectonique active de la Cordillère Blanche et du Callejon
492 de Huaylas (Andes nord-péruviennes), *Thèse présentée pour obtenir le grade de docteur,*
493 *Université de Paris-Sud, Centre d'Orsay*, 1–202.

494 Bott, M. (1959), The mechanics of oblique slip faulting, *Geol. Mag.*

495 Bussel, M.A. and W. S. Pitcher (1985), The structural control of batholith emplacement. In
496 *Magmatism at a Plate Edge, the Peruvian Andes,* edited by W.S. Pitcher, M.P. Atherton,
497 E. J. Cobbing and R.D. Beckinsale, pp. 167–176, Blackie Halstead Press, London.

498 Cobbing, J., W. Pitcher, J. Baldock, W. Taylor, W. McCourt, and N. J. Snelling (1981),
499 Estudio geológico de la Cordillera Occidental del norte del Perú, *Instituto Geologico*
500 *Minero y Metalurgico, Serie D. Estudios Especiales*, *10*(D), 1–252.

501 Dalmayrac, B., and P. Molnar (1981), Parallel thrust and normal faulting in peru and
502 constraints on the state of stress, *Earth and Planetary Sciences Letters*, *55*, 473–481.

503 Delvaux, D. (2012), Release of program Win-Tensor 4.0 for tectonic stress inversion:
504 statistical expression of stress parameters, *EGU General Assembly Conference Abstracts*.

505 Delvaux, D., and A. Barth (2010), African stress pattern from formal inversion of focal
506 mechanism data, *Tectonophysics*, *482*, 105–128, doi:10.1016/j.tecto.2009.05.009.

507 Delvaux, D., and B. Sperner (2003), New aspects of tectonic stress inversion with reference to
508 the TENSOR program, *Geological Society, London, Special Publications*, *212*(1), 75–
509 100, doi:10.1144/GSL.SP.2003.212.01.06.

510 Deverchère, J., C. Dorbath, and L. Dorbath (1989), Extension related to a high topography:
511 results from a microearthquake survey in the Andes of Peru and tectonic implications,
512 *Geophysical Journal International*, *98*(2), 281–292.

513 Dewey, J. F., and S. H. Lamb (1992), Active tectonics of the Andes, *Tectonophysics*, *205*(1),
514 79–95.

515 Divins, D. L. (2006), Total sediment thickness of the world's oceans and marginal seas,

516 Doser, D. I. (1987), The Ancash, Peru, earthquake of 1946 November 10: evidence for low-
517 angle normal faulting in the high Andes of northern Peru, *Geophysical Journal of the*
518 *Royal Astronomical Society*, *91*, 57–71.

519 Farber, D. L., G. S. Hancock (in prep), Tectonic and glacial forcing of motion along an active
520 detachment fault.

521 Folguera, A., T. Zapata, and V. A. Ramos (2006), Late Cenozoic extension and the evolution
522 of the Neuquén Andes, *Geological Society of America special papers*, *407*, 267–285.

523 Froidevaux, C., and B. L. Isacks (1984), The mechanical state of the lithosphere in the
524 Altiplano-Puna segment of the Andes, *Earth and Planetary Science letters*, *71*(2), 305–
525 314.

526 Gayet, M., L. G. Marshall, and T. Sempéré (1991), The Mesozoic and Paleocene vertebrates
527 of Bolivia and their stratigraphic context: a review, in Fósiles y Facies de Bolivia, edited by
528 R. Suárez, 12(3-4), 393–433.
529

530 Gérault, M., L. Husson, M. S. Miller, and E. D. Humphreys (2015), Flat‐slab subduction,
531 topography, and mantle dynamics in southwestern Mexico, *Tectonics*,
532 doi:10.1002/(ISSN)1944-9194.

533 Giovanni, M. K. (2007), Tectonic and Thermal Evolution of the Cordillera Blanca
534 Detachment System, Peruvian Andes: Implication for Normal Faulting in a
535 Contractionnal Orogen, 1–255 pp. University of California, Los Angeles.

536 Giovanni, M. K., B. K. Horton, C. N. Garzione, B. McNulty, and M. Grove (2010),
537 Extensional basin evolution in the Cordillera Blanca, Peru: Stratigraphic and isotopic
538 records of detachment faulting and orogenic collapse in the Andean hinterland, *Tectonics*,
539 *29*(6), TC6007, doi:10.1029/2010TC002666.

540 Gutscher, M. A., J. Malavieille, S. Lallemand, and J.-Y. Collot (1999), Tectonic segmentation
541 of the North Andean margin: impact of the Carnegie Ridge collision, *Earth and Planetary*
542 *Science letters*, *168*(3), 255–270.

543 Gutscher, M.-A., W. Spakman, H. Bijwaard, and E. R. Engdahl (2000), Geodynamics of flat
544 subduction: Seismicity and tomographic constraints from the Andean margin, *Tectonics*,
545 *19*(5), 814–833.

546 Hampel, A. (2002), The migration history of the Nazca Ridge along the Peruvian active
547 margin: a re-evaluation, *Earth and Planetary Science letters*, *203*(2), 665–679.

548 Heuret, A., F. Funiciello, C. Faccenna, and S. Lallemand (2007), Plate kinematics, slab shape
549 and back-arc stress: A comparison between laboratory models and current subduction
550 zones, *Earth and Planetary Science Letters*, *256*(3), 473-483.

551 Hodson, K. R. (2012), Morphology, exhumation, and Holocene erosion rates from a tropical
552 glaciated mountain range: the Cordillera Blanca, Peru, 1–94 pp. McGill University
553 Masters of science.

554 Jaillard, E. (1993), L'évolution tectonique de la marge péruvienne au Sénonien et Paleocène et
555 ses relations avec la géodynamique. *Bulletin-Société Géologique de France*, *164*, 819-
556 819.

557 Jaillard, E. (1994), Kimmeridgian to Paleocene tectonic and geodynamic evolution of the
558 Peruvian (and Ecuadorian) margin, In *Cretaceous tectonics of the Andes*, edited by J. A.
559 Salfity, pp. 101–167, Vieweg, Teubner Verlag.

560 Jaillard, E., and P. Soler (1996), Cretaceous to early Paleogene tectonic evolution of the
561 northern Central Andes (0–18°S) and its relations to geodynamics, *Tectonophysics*,

562 *259*(1), 41–53.

563 James, D. E. (1971), Plate tectonic model for the evolution of the Central Andes, *Geological*
564 *Society of America Bulletin*, *82*, 3325–3346.

565 Jordan, T. E., B. L. Isacks, R. W. Allmendinger, J. A. Brewer, V. A. Ramos, and C. J. Ando
566 (1983), Andean tectonics related to geometry of subducted Nazca plate, *Geological Study*
567 *of America Bulletin*, *94*, 341–361.

568 Kay, R. W., and S. M. Kay (2002), Andean adakites: three ways to make them, *Acta*
569 *Petrologica Sinica*.

570 Lacombe, O. (2012), Do fault slip data inversions actually yield ‘‘paleostresses’’ that can be
571 compared with contemporary stresses? A critical discussion, *Comptes Rendus*
572 *Geoscience*, *344*(3-4), 159–173, doi:10.1016/j.crte.2012.01.006.

573 Margirier, A., X. Robert, L. Audin, C. Gautheron, M. Bernet, S. Hall, and T. Simon-Labric
574 (2015), Slab flattening, magmatism and surface uplift in the Cordillera Occidental
575 (northern Peru), *Geology*, 1–4, doi:10.1130/G37061.1.

576 Margirier, A., L. Audin, X. Robert, F. Herman, J. Ganne and S. Schwartz (2016), Time and
577 mode of exhumation of the Cordillera Blanca batholith (Peruvian Andes), *Journal of*
578 *Geophysical Research: Solid Earth, 121*, doi:10.1002/2016JB013055.

579 Marrett, R., and R. W. Allmendinger (1990), Kinematic analysis of fault-slip data, *Journal of*
580 *Structural Geology*, *12*(8), 973–986.

581 Martinod, J., L. Husson, P. Roperch, B. Guillaume, and N. Espurt (2010a), Horizontal
582 subduction zones, convergence velocity and the building of the Andes, *Earth and*
583 *Planetary Science letters*, *299*(3-4), 299–309, doi:10.1016/j.epsl.2010.09.010.

584 McKee, E. H., and D. C. Noble (1982), Miocene volcanism and deformation in the western
585 Cordillera and high plateaus of south-central Peru, *Geological Society of America*
586 *Bulletin*, *93*(8), 657-662.

587 McNulty, B. A., and D. L. Farber (2002), Active detachment faulting above the Peruvian flat
588 slab, *Geology*, *30*(6), 567–570.

589 McNulty, B. A., D. L. Farber, G. S. Wallace, R. Lopez, and O. Palacios (1998), Role of plate
590 kinematics and plate-slip-vector partitioning in continental magmatic arcs: Evidence from
591 the Cordillera Blanca, Peru, *Geology*, *26*(9), 827–830.

592 Mégard, F. (1978), Etude géologique des Andes du Pérou central: Mémoire ORSTROM, 86.

593 Mégard, F. (1984), The Andean orogenic period and its major structures in central and
594 northern Peru, *Journal of the Geological Society*, *141*(5), 893–900.

595 Mégard, F., D. C. Noble, E. H. McKEE, and H. Bellon (1984), Multiple pulses of Neogene
596 compressive deformation in the Ayacucho intermontane basin, Andes of central Peru,
597 *Geological Society of America Bulletin*, *95*(9), 1108–1117.

598 Mukasa, S. B. (1984), Comparative Pb isotope systematics and zircon U-Pb geochronology
599 for the Coastal, San Nicolás and Cordillera Blanca Batholiths, Peru, PhD thesis,
600 University of California, Santa Barbara.

601 Müller, R. D., M. Sdrolias, C. Gaina, and W. R. Roest (2008), Age, spreading rates, and
602 spreading asymmetry of the world's ocean crust, *Geochem. Geophys. Geosyst.*, *9*(4), 1–
603 19, doi:10.1029/2007GC001743.

604 Noble, D. C., E. H. McKee, T. Mourier, and F. Mégard (1990), Cenozoic stratigraphy,
605 magmatic activity, compressive deformation, and uplift in northern Peru, *Geological*
606 *Society of America Bulletin*, *102*(8), 1105-1113.

607 Nocquet, J.-M. et al. (2014), Motion of continental slivers and creeping subduction in the
608 northern Andes, *Nature Geoscience*, *7*(4), 287–291, doi:10.1038/ngeo2099.

609 Ortner, H., F. Reiter, and P. Acs (2002), Easy handling of tectonic data: the programs
610 TectonicVB for Mac and TectonicsFP for Windows™, *Computers & Geosciences*,
611 *28*(10), 1193–1200.

612 Pardo-Casas, F., and P. Molnar (1987), Relative motion of the Nazca (Farallon) and South
613 American plates since Late Cretaceous time, *Tectonics*, *6*(3), 233–248.

614 Petford, N., and M. P. Atherton (1992), Granitoid emplacement and deformation along a
615 major crustal lineament: the Cordillera Blanca, Peru, *Tectonophysics*, *205*(1), 171–185.

616 Pêcher, A. et al. (2008), Stress field evolution in the northwest Himalayan syntaxis, northern
617 Pakistan, *Tectonics*, *27*(6), n/a–n/a, doi:10.1029/2007TC002252.

618 Ramos, V. A., and A. Folguera (2009), Andean flat-slab subduction through time, *Geological*
619 *Society, London, Special Publications*, *327*(1), 31–54, doi:10.1144/SP327.3.

620 Ramos, V. A., E. O. Cristallini, and D. J. Pérez (2002), The Pampean flat-slab of the Central
621 Andes, *Journal of South American Earth Sciences*, *15*(1), 59–78.

622 Rosenbaum, G., D. Giles, M. Saxon, P. G. Betts, R. F. Weinberg, and C. Duboz (2005),
623 Subduction of the Nazca Ridge and the Inca Plateau: Insights into the formation of ore
624 deposits in Peru, *Earth and Planetary Science letters*, *239*(1-2), 18–32,
625 doi:10.1016/j.epsl.2005.08.003.

626 Ruff, L. J. (1989), Do trench sediments affect great earthquake occurrence in subduction
627 zones? *Subduction Zones Part II*, *129*(1-2), 264–282.

628 Ruff, L. J., and H. Kanamori (1983), Seismic coupling and uncoupling at subduction zones,
629 *Tectonophysics*, *99*(2-4), 99–117.

630 Saillard, M., L. Audin, B. Rousset, J. P. Avouac, M. Chlieh, S. R. Hall, L. Husson, and D. L.
631 Farber (2017), From the seismic cycle to long-term deformation: linking seismic coupling
632 and Quaternary coastal geomorphology along the Andean megathrust, *Tectonics*, *36*(2),
633 241–256, doi:10.1029/2002JB002072.

634 Schellart, W. P. (2008), Overriding plate shortening and extension above subduction zones: A
635 parametric study to explain formation of the Andes Mountains, *Geological Society of*
636 *America Bulletin*, *120*(11-12), 1441-1454.

637 Scheuber, E., and G. Gonzalez (1999), Tectonics of the Jurassic- Early Cretaceous magmatic
638 arc of the north Chilean Coastal Cordillera (22°-26°S): A story of crustal deformation
639 along a convergent plate boundary, *Tectonics*, *18*(5), 895‑910.

640 Schwartz, D. P. (1988), Paleoseismicity and neotectonics of the Cordillera Blanca fault zone,

641 northern Peruvian Andes, *Journal of Geophysical Research*, *93*(B5), 4712–4730.

642 Sébrier, M., J. L. Mercier, J. Macharé, D. Bonnot, J. Cabrera, and J. L. Blanc (1988), The
643 state of stress in an overriding plate situated above a flat slab: The Andes of Central Peru,
644 *Tectonics*, *7*(4), 895–928.

645 Siame, L. L., M. Sébrier, O. Bellier, and D. Bourles (2006), Can cosmic ray exposure dating
646 reveal the normal faulting activity of the Cordillera Blanca Fault, Peru? *Revista de la*
647 *Asociación Geológica Argentina*, *61*(4), 536–544.

648 Silgado, E. F. (1992), *Investigaciones de sismicidad histórica en la América del Sur en los*
649 *siglos XVI, XVII, XVIII y XIX*, Consejo Nacional de Ciencia y Tecnología, Lima.

650 Somoza, R. (1998), Updated Nazca (Farallon)—South America relative motions during the
651 last 40 My: implications for mountain building in the central Andean region, *Journal of*
652 *South American Earth Sciences*, *11*(3), 211–215.

653 Soulas, J. P. (1977), Las fases tectonicas del Terciario Superior en Peru-corte Ayacucho-
654 Pisco, *Boletin Sociedad Geológica del Perú*, 57-58.

655 Sperner, B., L. Ratschbacher, and R. Ott (1993), Fault-striae analysis: a Turbo Pascal program
656 package for graphical presentation and reduced stress tensor calculation, *Computers &*
657 *Geosciences*, *19*(9), 1361–1388.

658 Steinmann, G. (1929), Geologie von Peru, In *Heidelberg*, edited by K. Winter, pp. 448.

659 Stewart, J. W., J. F. Evernden, and N. J. Snelling (1974), Age determinations from Andean
660 Peru: a reconnaissance survey, *Geological Society of America Bulletin*, *85*(7), 1107–1116.

661 Taylor, G. K., J. Grocott, A. Pope, and D. E. Randall (1998), Mesozoic fault systems,
662 deformation and fault block rotation in the Andean forearc: a crustal scale strike-slip
663 duplex in the Coastal Cordillera of northern Chile, *Tectonophysics*, *299*(1), 93–109.

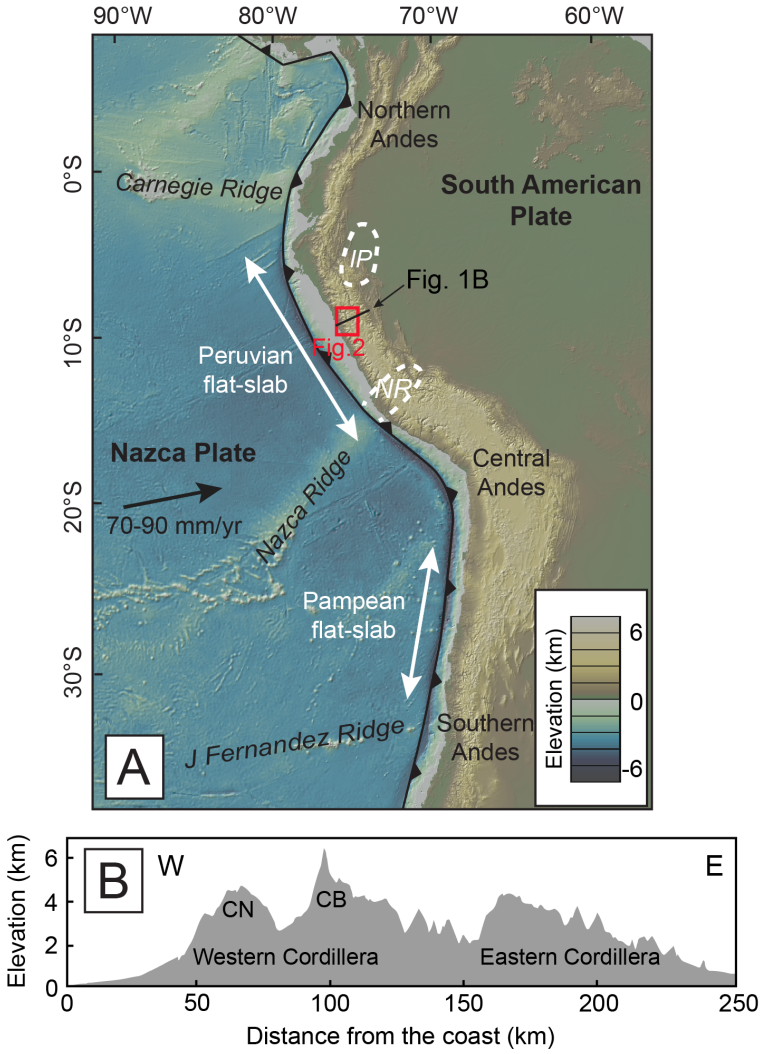
664 Wallace, R. E. (1951), Geometry of shearing stress and relation to faulting, *The journal of*
665 *Geology*, 118–130.

666 Wipf, M. (2006), Evolution of the Western Cordillera and Coastal Margin of Peru: Evidence
667 from low-temperature Thermochronology and Geomorphology, 1–163 pp. Swiss Federal
668 Institute of Technology Zürich, 7 March.

669 Wise, J. M., and D. C. Noble (2003), Geomorphic evolution of the Cordillera Blanca,
670 Northern Peru, *Boletin de la sociedad Geologica del Peru*, *96*, 1–21.

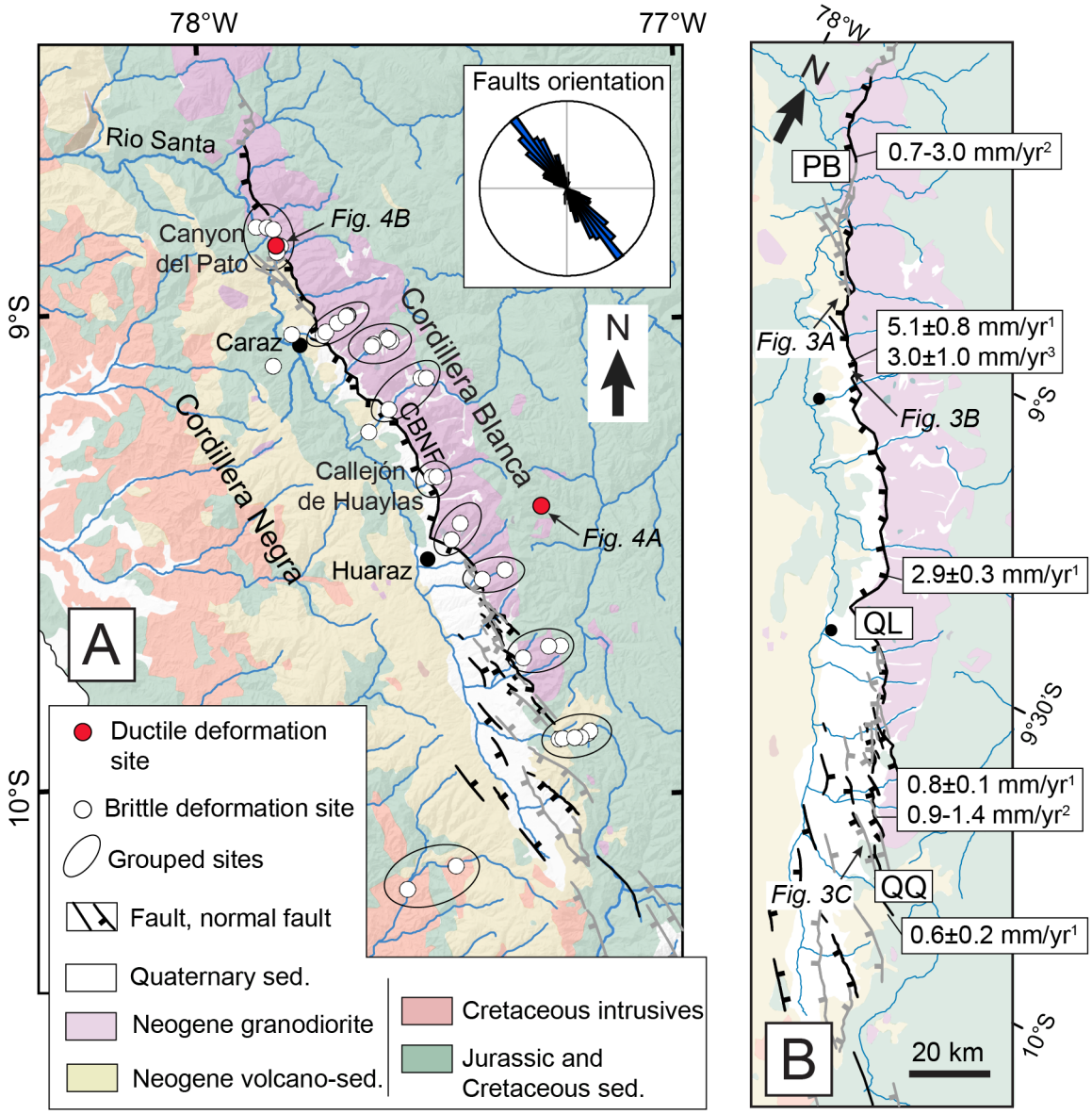
671 Yamaji, A. (2000), The multiple inverse method: a new technique to separate stresses from
672 heterogeneous fault-slip data, *Journal of Structural Geology*, *22*(4), 441–452,
673 doi:10.1016/S0191-8141(99)00163-7.

674 Zeilinger, G., J. P. Burg, N. Chaudhry, H. Dawood and S. Hussain (2000), Fault systems and
675 Paleo-stress tensors in the Indus Suture Zone (NW Pakistan), *Journal of Asian Earth*
676 *Sciences, 18*, 547-559.



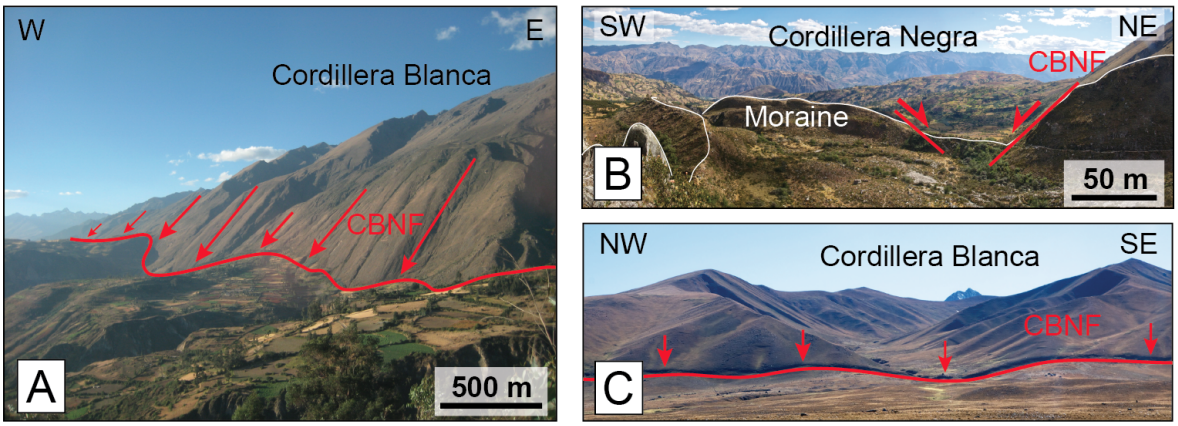
677

678 Figure 1: A) Topographic map of the Andes (SRTM data) including flat slab segments and
679 bathymetric features as the Nazca Ridge (NR) and the Inca plateau (IP; Inca Plateau location
680 after *Gutscher et al.* (1999)). The study area is indicated by the red rectangle. B) Topographic
681 cross-section of the Peruvian Andes at the latitude of the Cordillera Blanca showing the
682 Cordillera Blanca (CB), the Cordillera Negra (CN), the Western Cordillera and the Eastern
683 Cordillera.



684

685 Figure 2: Geological maps of the study area. A) Map showing the active faults mapped in this
686 study (black lines) and from Neotectonic Open Database (grey lines), the measurement
687 stations (white dot), the grouped sites and the sites where ductile deformation was analyzed
688 (red dot). Inset shows a rose diagram of the fault segments azimuth B) Zoom on the CBNF
689 with Quaternary vertical slip-rates from [1]*Farber and Hancock* (in prep), [2]*Schwartz* (1988) and
690 [3]*Siame et al.* (2006) and location of bedrock slickensides measurement sites along the CBNF
691 (Pachma Bajo, PB; Quebrada Llaca, QL and Quebrada Querococha, QQ).



692

693 Figure 3: Photographs of the CBNF. See the Figure 2B for locations. A) Triangular facets in
694 the northern part of the Cordillera Blanca (1000 m high). B) Moraine offset at the outlet of the
695 Quebrada Huaytapallana (offset ~100 m). C) Quaternary scarp in the Lloclla Formation
696 (southern Cordillera Blanca) (offset ~4 m).

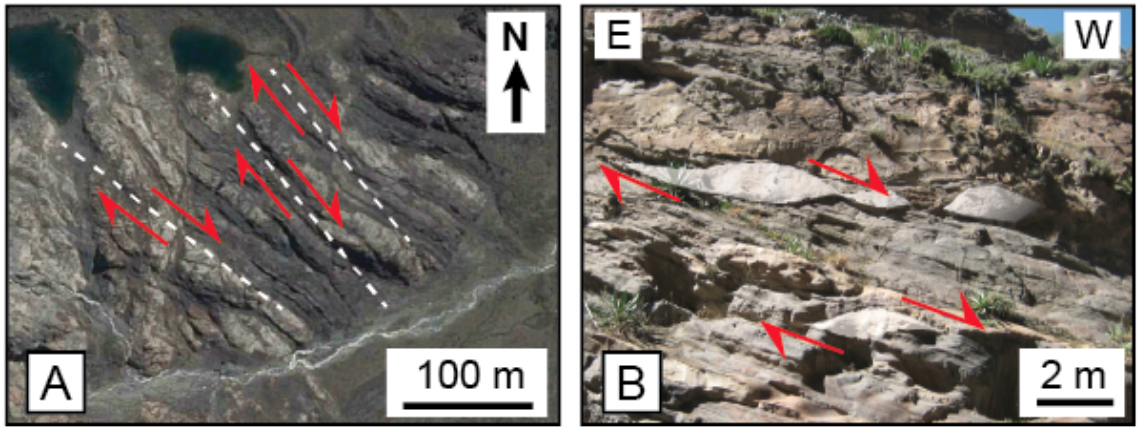
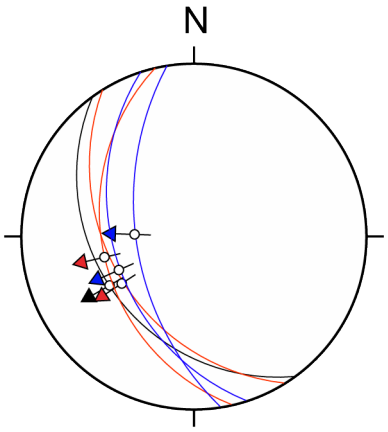
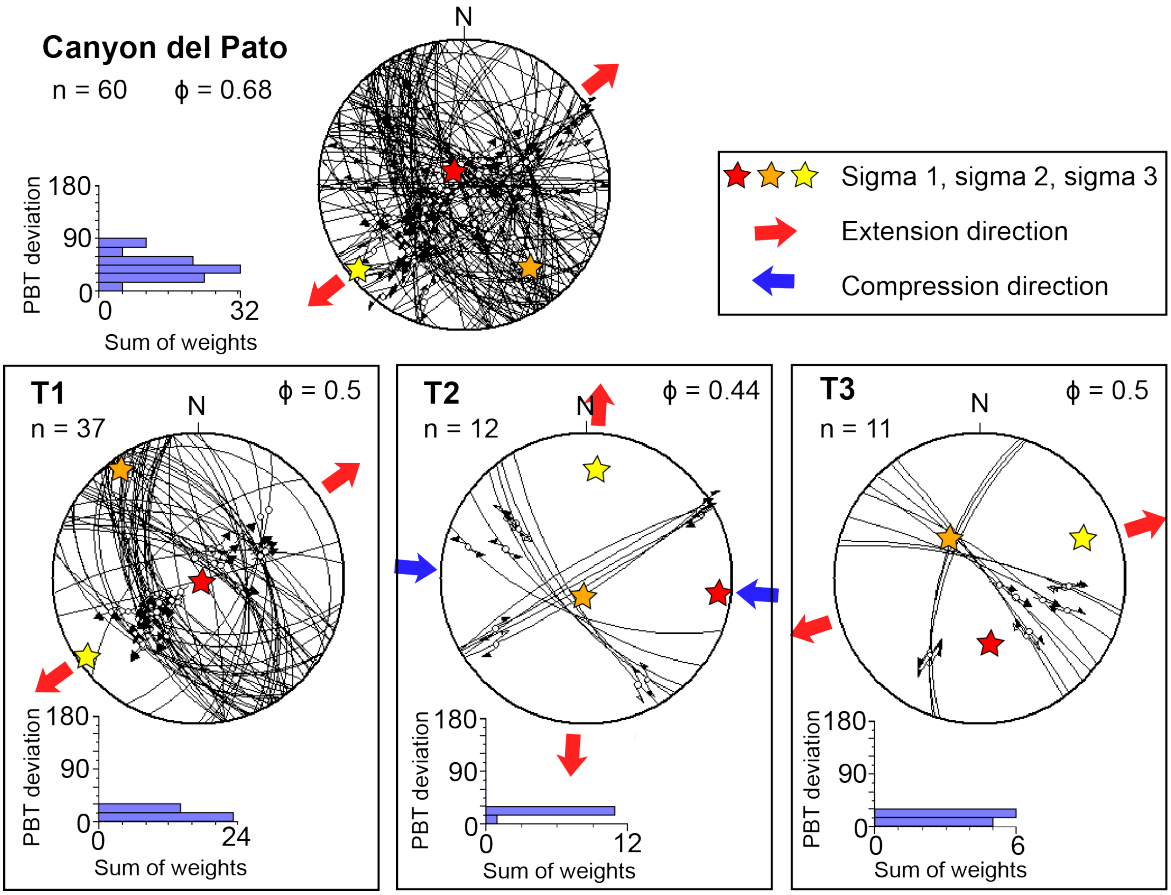


Figure 4: Ductile deformation in the Cordillera Blanca (see Figure 2 for location). A) Google Earth Landsat image with dextral strike-slip in the eastern Cordillera Blanca, about 20 km East from the CBNF. B) Photograph of the ductile deformation of dykes in the cliffs of the Canyon del Pato, in the CBNF zone.



703

704 Figure 5: Cordillera Blanca fault planes and striaes orientation and dip, Wulff lower
705 hemisphere stereographic projection. Measurements were done in Pachma Bajo (PB; blue),
706 Quebrada Llaca (QL; black) and Quebrada Querococha (QQ; red), see figure 2B for the
707 location of the sites.



708

709 Figure 6: Faults in the Canyon del Pato (Cordillera Blanca), Wulff lower hemisphere
710 stereographic projection. A) All faults measurements and associated tensor calculation (PBT
711 method) the angular deviation is shown by the histogram, *n* corresponds to the number of
712 fault measurements for each tensor, *Phi* corresponds to a shape parameter defined here as *Phi*
713 = $(\sigma_2 - \sigma_3)/(\sigma_1 - \sigma_3)$. B-D) Tensors T1, T2, T3 and related fault-slickenline pairs (see text for
714 tensor determination method).

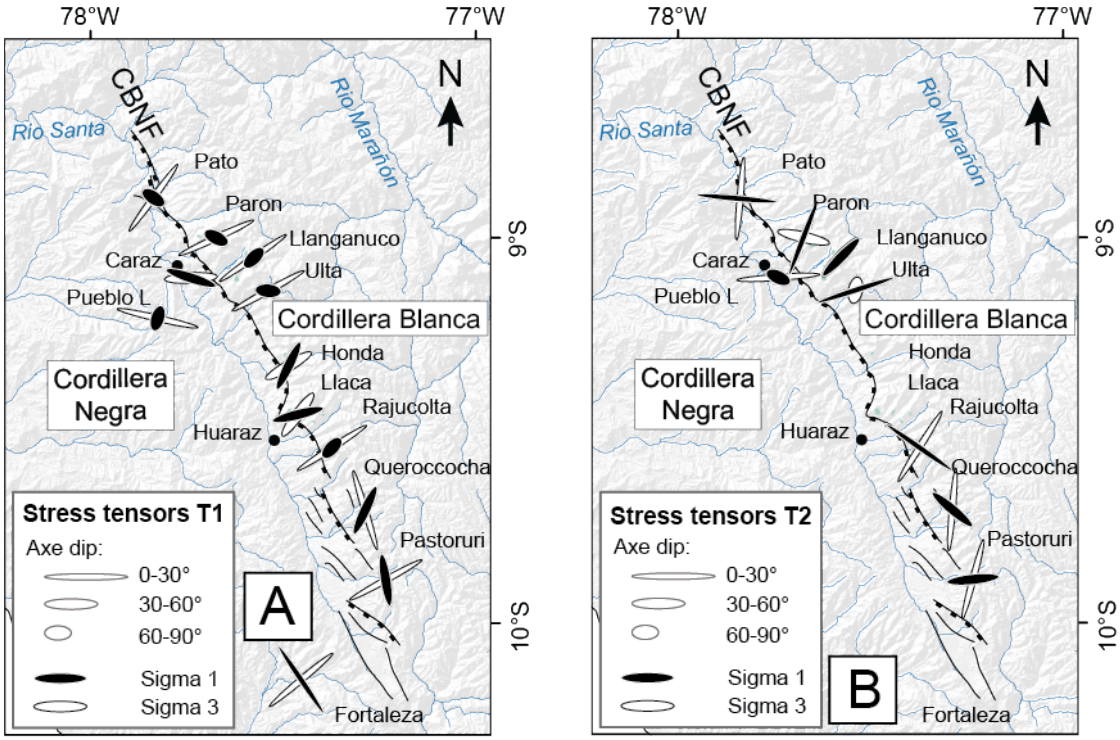
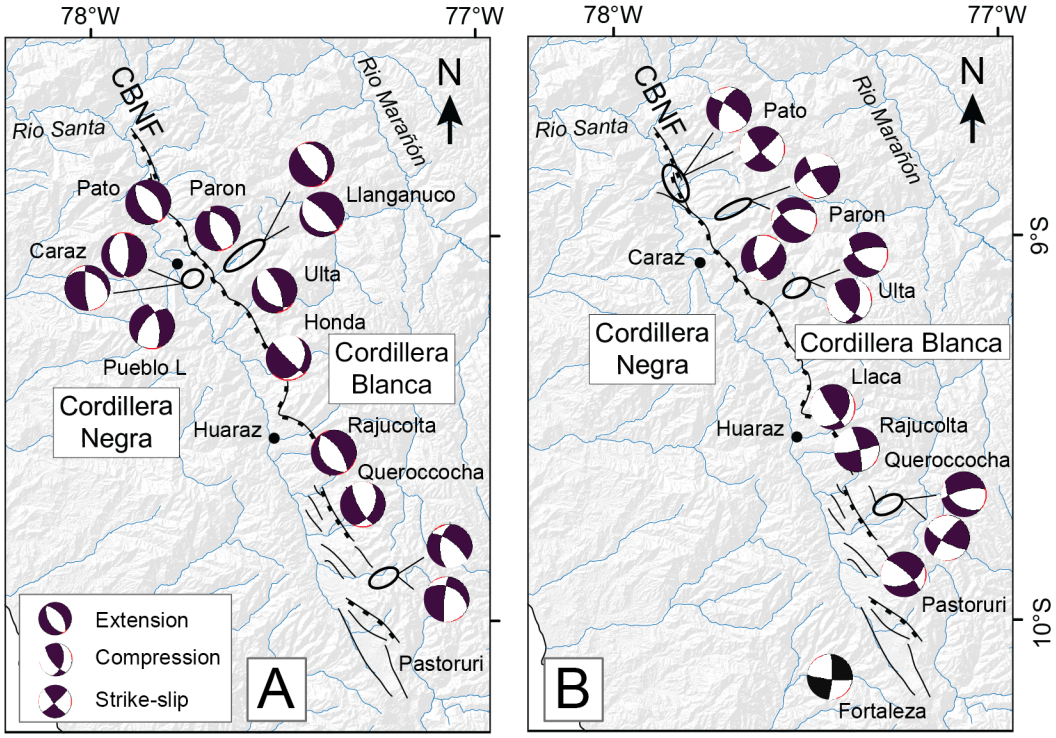


Figure 7: Stress orientation for grouped sites in the Cordillera Blanca region. Stress tensors were calculated using all the fault-slickenline pairs available in one region. Ellipses represents the stress (σ_1 in black, σ_3 in white), the direction of the ellipse great axis corresponds to the azimuth of the stress axis; the shape of the ellipse gives the plunge. The two best stress tensors are shown on the maps. A) Stress tensors T1, B) Stress tensors T2.



721

722 Figure 8: Stress tensors for grouped stations. A) Stress tensors corresponding to the present
723 day regional stress tensor (NE-SW extension) inferred from microearthquakes survey
724 (*Deverchère et al.*, 1989). B) Other stress tensors recorded by the brittle deformation.

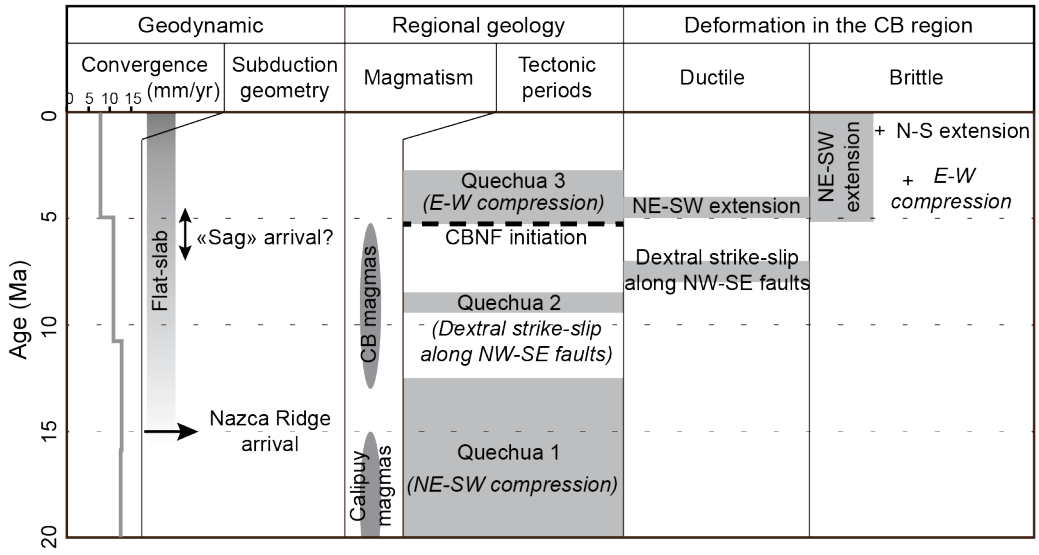


Figure 9: Schematic table that summarizes the northern Peru geodynamic events, regional geology and results of stress field analyzes for the past 20 Ma. The table includes the mean convergence rate (*Somoza*, 1998), subduction geometry (*Barazangi and Isacks*, 1976; *Gutscher et al.*, 1999; *Rosenbaum et al.*, 2005; *Margirier et al.*, 2015), magmatism age (e.g., *Cobbing et al.*, 1981; *Mukasa*, 1984; *Beckinsale et al.*, 1985), tectonic phases (e.g., *Mégard,* 1984) and our ductile and brittle deformation results.

Table 1
Stress tensors from grouped sites.

Site	Tensor	Number of couples fault/striation	PBT				Right diedra			
			Phi	Sigma 1	Sigma 3	Maximum angular deviation (°)	Phi	Sigma 1	Sigma 3	Maximum angular deviation (°)
Canyon del Pato		**128**								
	T1	66	0.53	85/146	01/234	30	0.51	77/149	00/058	30
	T2	12	0.44	04/095	15/005	28	0.42	15/090	11/357	32
	T3	11	0.50	38/171	14/068	29	0.64	42/181	25/066	25
Caraz		**34**								
	T1	9	0.53	53/108	31/251	33	0.67	54/106	33/259	24
	T2	10	0.58	66/295	20/086	34	0.55	62/328	19/099	34
	T3	8	0.70	07/265	74/165	42	0.69	00/264	67/174	30
Pueblo Libre		**12**								
	T1	12	-	-	-	-	0.62	61/197	02/103	30
Laguna Paron		**60**								
	T1	15	0.48	72/117	12/245	33	0.32	65/124	17/255	27
	T2	16	0.45	12/201	31/103	34	0.44	10/194	31/098	30
	T3	6	0.51	56/085	14/197	26	0.67	60/081	17/202	26
Quebrada Llanganuco		**58**								
	T1	23	0.50	65/045	25/235	34	0.56	59/104	17/226	43
	T2	8	0.50	52/010	06/109	32	0.56	58/006	07/108	32
Quebrada Ulta		**63**								
	T1	27	0.50	70/275	17/061	33	0.56	66/282	17/053	35
	T2	13	0.49	12/252	62/011	30	0.46	07/258	79/027	32
	T3	6	0.50	52/112	10/011	29	0.50	61/103	10/355	37
Quebrada Honda		**15**								
	T1	9	0.44	50/026	32/240	31	0.25	43/033	39/254	26
Quebrada Llaca		**14**								
	T1	6	0.50	32/256	50/036	27	0.67	01/123	56/031	44
Quebrada Rajucolta		**21**								
	T1	7	0.50	76/223	14/057	24	0.57	69/225	21/058	35
	T2	7	0.56	16/305	04/212	24	0.57	13/303	09/211	19
Quebrada Queroccocha		**70**								
	T1	15	0.50	59/025	24/163	30	0.47	68/032	18/251	39
	T2	16	0.44	59/130	19/005	32	0.34	67/146	16/013	32
	T3	8	0.61	05/346	27/080	30	0.62	12/346	28/083	25
	T4	6	0.54	07/041	10/133	33	0.67	04/229	22/137	31
Quebrada Pastoruri		**89**								
	T1	25	0.57	57/171	11/061	34	0.60	52/162	12/056	31
	T2	16	0.46	50/264	18/015	33	0.50	35/258	29/011	33
	T3	6	0.63	46/125	29/232	28	0.75	50/123	30/257	21
Fortaleza Valley		**14**								
	T1	7	0.55	17/326	00/230	35	0.50	31/312	06/046	38